Wave-front Behaviour of the Pulsed EM Field – Complexity and Implications

Gu, Junhong ; Neto, Andrea; Lager, Ioan E.; Stumpf, Martin

Citation (APA)
Gu, J., Neto, A., Lager, I. E., & Stumpf, M. (2023). Wave-front Behaviour of the Pulsed EM Field – Complexity and Implications. In *Proceedings of the 2023 17th European Conference on Antennas and Propagation (EuCAP)* (pp. 1-5). (17th European Conference on Antennas and Propagation, EuCAP 2023). IEEE. https://doi.org/10.23919/EuCAP57121.2023.10132997

Important note
To cite this publication, please use the final published version (if applicable).
Please check the document version above.

Wave-front Behaviour of the Pulsed EM Field – Complexity and Implications

Junhong Gu*, Andrea Neto*, Ioan E. Lager*, and Martin Štumpf[†],
*Terahertz Sensing Group, Faculty of Electrical Engineering, Mathematics and Computer Science,
Delft University of Technology, 2628 CD Delft, the Netherlands,
j.gu-3@student.tudelft.nl, a.neto@tudelft.nl, i.e.lager@tudelft.nl
[†]Lerch Laboratory of EM Research, Dept. Radioelectronics, Faculty of Electrical Engineering and Communication,
Brno University of Technology, Technická 3082/12, 616 00 Brno, The Czech Republic, martin.stumpf@centrum.cz

Abstract—The pulsed electromagnetic (EM) field radiated by a gap-fed, long slot in a perfectly conducting thin sheet located in between dielectric and free-space subdomains is examined. A phenomenological interpretation of the so-called head wave (HW) constituent is proposed, this fostering the understanding of the complex EM behaviour at, and immediately behind, the HW wave-front. The EM field is also examined numerically for identifying features that may lead the way towards inferring a causal counterpart of the leaky-wave propagation.

I. INTRODUCTION

The last two decades evidenced a surge in the interest for leaky-wave antennas (LWAs) within the antenna engineering community. This situation stems from LWAs being recognised as critical enablers for implementing the ultra-high data rate and low latency required by digital communications (see [1] for the physical layer requirements in present and upcoming, 6G networks). Although variants exist, LWAs come in two main classes of implementations: (i) making use of the propitious electromagnetic (EM) field distributions associated with the guided propagation along interfaces between two media [2]–[8] or (ii) making use of periodic structures the EM radiation from which replicates that from Fabry-Pérot cavities [9]–[13]. This study focuses on the former class, with all presented arguments explicitly assuming such structures.

The design of LWAs requires a thorough understanding of the EM field distribution associated with the underlying (canonical) structures. In this respect, [14], [15] give an excellent overview on the vast range of theoretical studies on leaky-wave (LW) propagation – from them, [16], [17] are singled out for being conditional for the reasoning in this study. The remarkable common denominator of these methods is that they *all* perform the analysis in the frequency-domain (FD), with strictly time-domain (TD) examinations being literally absent (at least in the overviews [14], [15]). It is exactly this loophole that the present account attempts to address.

The TD analysis of planar layered media of the kind that underpin LWAs has a long history, with the Cagniard–de Hoop (**C-dH**) technique [18], [19], justifiably being regarded as the instrument of choice to this end. Following this, or similar paths (see [20, Chapter 2]), allows establishing via rigorous spectral-domain arguments that the pulsed-field EM propagation in such layered media comprises two *causal* wave constituents, namely the *body waves* (BW) and the *head waves* (HW), the latter existing only in regions of space located beyond the critical angle associated with a given planar interface (when such a critical angle applies). A detailed inspection of the conditions under which these causal constituents propagate has been provided in [21].

However, such rigorous theoretical TD results can only be derived for a reduced set of canonical problems. In particular, no analytic framework exists for a gap-fed, long slot in a perfectly conducting (PEC) thin sheet at the planar interface bewteen dielectric and free-space subdomains (although the **C-dH** Method of Moments [22] may bring about the needed conceptual step forward). Such a slot is the basic configuration supporting the functioning of the leaky-lens antenna (LLA) introduced in [2], a device that established itself as a reference for the (sub-)terahertz, non-dispersive EM transfer.

This study is a first step towards understanding the pulsed-field EM propagation from a the gap-fed, long slot. After recapitulating the formal definition of BW and HW constituents, it will propose a phenomenological interpretation of the HW constituent that facilitates the understanding of the complex EM behaviour at, and immediately behind, the HW wave-front. TD numerical experiments effectuated via CST Studio Suite® (CST Studio) will then highlight some features that pave the way towards a *causal counterpart* of the LW propagation. The study is complemented with two appendices elaborating on (numerical) instruments that play a prominent role in the paper.
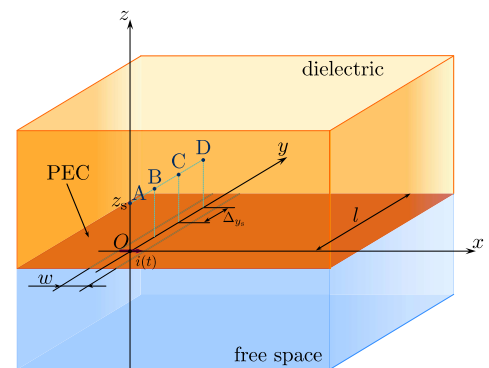

Fig. 1. Examined two-media configuration. In the numerical experiments: $\varepsilon_{\mathrm{r}} = 16$, $w = 1\,\mathrm{mm}$, $l = 40\,\mathrm{mm}$, $z_{\mathrm{s}} = 1\,\mathrm{mm}$ and $\Delta_{y_{\mathrm{s}}} = 4\,\mathrm{mm}$.

II. EXAMINED CONFIGURATION

The configuration at the core of the present study is shown in Fig. 1. In it, position is specified with respect to a Cartesian reference frame with origin O and three mutually orthogonal unit vectors $\{\boldsymbol{i}_x, \boldsymbol{i}_y, \boldsymbol{i}_z\}$. The time coordinate is t. Position vectors are denoted as $\boldsymbol{r} = x\boldsymbol{i}_x + y\boldsymbol{i}_y + z\boldsymbol{i}_z$. The configuration consists of two half-spaces, the one corresponding to $z < 0$ being taken to be free space with permittivity ε_0 and permeability μ_0, while the one corresponding to $z > 0$ being occupied by a lossless dielectric with permittivity $\varepsilon_1 = \varepsilon_{\mathrm{r}}\varepsilon_0$ and permeability μ_0. The wavespeeds in any of the two half-spaces are $c_{0,1} = (\varepsilon_{0,1}\mu_0)^{-\frac{1}{2}}$ and the wave impedances are $Z_{0,1} = (\mu_0/\varepsilon_{0,1})^{\frac{1}{2}}$. The interface between the half-spaces is occupied by a PEC sheet of vanishing thickness in which a long slot of width w is cut, its position being symmetrical with respect to the Oy-axis. The slot is fed by a current-source-type port located along the Ox-axis that injects a time-windowed current pulse $i(t)$. The slot is, theoretical, infinitely long, but its length will be truncated to l in numerical evaluations.

Since it focuses on conceptual progress, this study is deliberately confined to lossless dielectric media, which was also the strategy in [2], [16]. Accounting for these technologically unavoidable effects is deferred to future research.

III. WAVE CONSTITUENTS IN THE EXAMINED CONFIGURATION

A. Wave constituent definitions based on EM spectral representation

As indicated in the Introduction, the considered configuration is optimally analysed by applying the **C-dH** technique. This method requires transforming the TD field equations via a unilateral Laplace transform with positive, real parameter s, combined with a spatial Fourier representation translating the problem into the slowness domain (see [23, Chapter 2] for details). After solving the problem in the slowness domain, the solution is expressed as a superposition of generalised rays in the Laplace domain that, in turn, are transformed back to the TD via a suitable contour deformation. The spectral-domain analysis of the solution allows discerning between two types of constituents:

- body waves (BWs) that always exist;
- head waves (HWs) that only arise at an incidence above the critical angle ϑ_{c} associated with a given (planar) interface, when such a critical angle is of relevance.

The user is referred to [23, Chapter 2] for the treatment of these constituents. An important element is their arrival time at a field point. Consider the configuration in Fig. 2.a – the depicted situation concurs with the one occurring in the $x = 0$ plane in Fig. 1. Assume, for simplicity, that this configuration is excited by a line source $\mathcal{S}$ located along the $y = 0$ axis. Take now a point $\mathcal{P}$ that corresponds to an incidence at an angle exceeding the critical angle

$$y/(y^2 + h^2)^{\frac{1}{2}} > \sin(\vartheta_{\mathrm{c}}) = c_1/c_0 = 1/\sqrt{\varepsilon_{\mathrm{r}}}. \quad (1)$$

The applicable arrival times are (see Eqs. (9) and (14) in [24])

$$\tau_{\mathrm{a;BW}} = (y^2 + h^2)^{\frac{1}{2}}/c_1 \quad (2)$$

$$\tau_{\mathrm{a;HW}} = y/c_0 + h\left(c_1^{-2} - c_2^{-2}\right)^{\frac{1}{2}} = c_0^{-1}\left(y + h\sqrt{\varepsilon_{\mathrm{r}} - 1}\right) \quad (3)$$
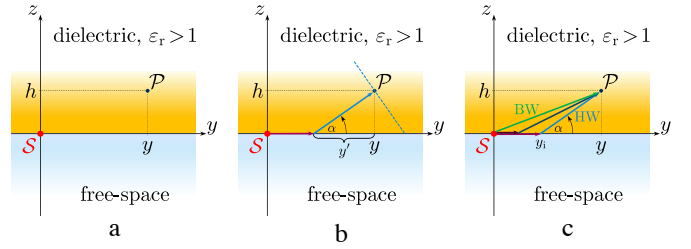
for the BW and HW, respectively.

Fig. 2. Explicative for the propagation of the wave constituents. (a) Cross-section through a two-media configuration – representative for the situation in the plane $x = 0$ in Fig. 1; (b) the HW path segments and the HW wave-front; (c) BW and HW paths connecting the source $\mathcal{S}$ and the field point $\mathcal{P}$.

B. Phenomenological introduction of the head-waves

While the formal treatment of the two constituents in the spectral domain offers the needed rigor, a phenomenological introduction of the HWs fosters their interpretation, especially in those cases when their complete spectral handling is difficult, if at all possible.

The physical interpretation of the HW is that of the first EM field disturbance propagating away from $\mathcal{S}$ and sensed at $\mathcal{P}$ – the path of this ray is sketched in Fig. 2.b. To understand this, one must recall that EM waves start from the source and travel in free-space at the wavespeed c_0 and in the dielectric at the wavespeed $c_1 = c_0/\sqrt{\varepsilon_{\mathrm{r}}} < c_0$. The wave front propagating faster in the free-space will produce secondary sources at the interface which, in turn, will radiate into the dielectric – those waves will reach some points inside the dielectric ahead of *any* wave propagating exclusively through the dielectric. With this in mind, the HW is the wave that, by combining propagation along the interface and through the dielectric, minimises the travel time between $\mathcal{S}$ and $\mathcal{P}$. The travel time τ along that path will then be (see Fig. 2.b)

$$\tau = c_0^{-1}(y - y') + c_1^{-1}(y'^2 + h^2)^{\frac{1}{2}} = c_0^{-1}\mathscr{F}(y'). \quad (4)$$

By now taking the derivative of $\mathscr{F}(y')$ and equating it to zero it is found that the relevant y' is

$$y' = h/\sqrt{\varepsilon_{\mathrm{r}} - 1} \quad (5)$$

that, when substituted back into (4), will yield the minimum time the wave takes from $\mathcal{S}$ and $\mathcal{P}$ namely

$$\tau_{\min} = c_0^{-1}\left(y + h\sqrt{\varepsilon_{\mathrm{r}} - 1}\right) = \tau_{\mathrm{a;HW}}. \quad (6)$$

It was thus shown that the indicated path corresponds, indeed, to the HW path. It should also be observed that the angle at which the HW propagates through the dielectric is

$$\alpha = \arctan(h/y') = \arctan\left(\sqrt{\varepsilon_{\mathrm{r}} - 1}\right) \quad (7)$$

in which (5) was used. Furthermore, the wavefront of the HW is formed by all points at which the WH arrives at the same time which, from (3), corresponds to the line

$$z = (-y + c_0\,\tau_{\mathrm{a;HW}})/\sqrt{\varepsilon_{\mathrm{r}} - 1} \text{ for } z > 0 \quad (8)$$

which demonstrates (as expected) that the wavefront is orthogonal to the direction defined in (7).

The HW path provides the fastest path for a disturbance to travel from $\mathcal{S}$ to $\mathcal{P}$. With reference to Fig. 2.c, any other path, comprising a shorter segment along the interface, will yield a longer propagation time between $\mathcal{S}$ and $\mathcal{P}$ – an example of such a path is the one shown in dark plum and dark blue. The slowest path is the direct path, corresponding to the BW – this path is marked in Fig. 2.c in green.

Assume now that the feeding signal at $\mathcal{S}$ is not only *causal* but also *continuous*. Such a feeding will then necessarily be just marginally non-vanishing immediately after its onset. As a result, it is clear that the signal level at the wave-front arriving at $\mathcal{P}$ at $\tau_{\mathrm{a;HW}}$ must be extremely low. At subsequent instants $\tau_{\mathrm{a;HW}} + \Delta_t$, with $\Delta_t < \tau_{\mathrm{a;BW}} - \tau_{\mathrm{a;HW}}$, the effect of later (presumably, stronger) parts of the feeding signal will arrive at $\mathcal{P}$ via the HW path. Concomitantly, the effect of previous parts of the signal will also arrive at $\mathcal{P}$ via increasingly slow paths (akin of the intermediate path in Fig. 2.c). Moreover, even the effect of secondary sources located at points *beyond* y along the interface may be sensed at $\mathcal{P}$. It is now evident that the aggregate field at $\mathcal{P}$ follows as the superposition of a multitude of propagating rays that is likely to produce both field enhancements and nulls. In any event, that aggregate effect contains *no* BW contributions.

This analysis demonstrates the complexity of the radiated EM field in the region *preceding* the arrival of the BW. The field modulation in the vicinity of the interface, without itself propagating, is bound to have an effect in the far-field. With this in mind [24] identified (truly, for a slightly different situation) an EM field peak between $\tau_{\mathrm{a;HW}}$ and $\tau_{\mathrm{a;BW}}$ that was shown to present remarkable similarities with features that are specific to leaky-waves (LW), the arrival time of that extremum being [24, Eq. (25)]

$$\tau_{\mathrm{a;LW}} = |y|/\sqrt{2}(c_1^{-2} + c_0^{-2})^{\frac{1}{2}} + z/\sqrt{2}(c_1^{-2} - c_0^{-2})^{\frac{1}{2}}. \quad (9)$$

IV. NUMERICAL STUDY OF THE EM PROPAGATION AT THE WAVE-FRONT

The temporal behaviour of the EM field at the 4 points in the $x = 0$ plane of the configuration in Fig. 1 was examined via simulations performed by means of CST Studio Suite®. The emphasis was on the interval between the arrival of the HW and BW constituents. The slot width was $w = 0.5\,\mathrm{mm}$ and the relative permittivity in the dielectric was $\varepsilon_{\mathrm{r}} = 16$. The excitation was taken as the triangular pulse in Fig. 3. The domain of computation was large enough in the x and y directions for preventing, within the investigated time interval, any boundary reflections inside the spatial domain of interest ($l = 40\,\mathrm{mm} \gg s_{\mathrm{w}} > w$). Transparent (PML) conditions were prescribed above and below. The simulated signatures were

smoothed via a moving average over 5 consecutive points and were time-calibrated such that their onset corresponded to $\tau_{\mathrm{a;BW}}$ at A (where only BWs exist) and to $\tau_{\mathrm{a;HW}}$ at B, C and D (where HWs are also intercepted). The resulting signatures are shown in Fig. 4 in which the time markers for $\tau_{\mathrm{a;BW}}$ and $\tau_{\mathrm{a;HW}}$ (when applicable) are given. Furthermore, time markers for $\tau_{\mathrm{a;LW}}$ in (9) are also included, when applicable.
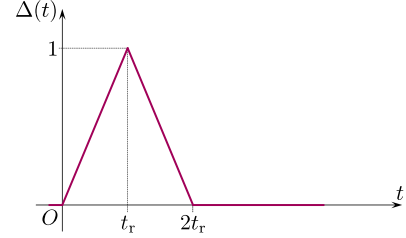

Fig. 3. The employed triangular pulse $\Delta(t)$. Its pulse width was $t_{\mathrm{w}} = 2t_{\mathrm{r}} = 5\,\mathrm{ps}$, this entailing a spatial pulse extent $s_{\mathrm{w}} = c_0 t_{\mathrm{w}} = 1.5\,\mathrm{mm}$.

A. Numerical determination of the impulse response

For properly examining the EM field behaviour, the configurational impulse response at points A,...,D was extracted from the signatures in Fig. 4 via Matlab post-processing. To this end, the Matlab native `deconv` and an original, Laplace-transform strategy (see Appendix A) were employed. The deconvolved signatures were also smoothed and time-calibrated as indicated above. The deviation between the original (simulated) and deconvolved signatures is discussed in Appendix B allowing to conclude that, for the employed excitation, the original signatures can be safely construed as the configurational impulse responses at the field points.

B. Interpretation of the numerical results

The examination of the plots in Fig. 4 allows establishing a number of conclusions concerning the calculated signatures. To begin with, the signature at A contains, as expected, BW constituents, only. While the directly yielded information is minimal, it allows verifying and calibrating the subsequent signatures. When moving to the points B, C and D, it is clear that some interesting features become visible. In this respect, it is important to note that the lower lobe expands steadily when moving away from the source as a result of the increasingly long interval between $\tau_{\mathrm{a;HW}}$ and $\tau_{\mathrm{a;BW}}$. Moreover, the lowermost point on the signatures moves increasingly closer to the $\tau_{\mathrm{a;LW}}$ marker, which concurs with the observation made in [24] that this is an extremum in the EM field radiated in the interval $t \in (\tau_{\mathrm{a;HW}}, \tau_{\mathrm{a;BW}})$. To conclude with, no specific feature could be identified around $\tau_{\mathrm{a;BW}}$ that is illustrative for the fact that, unlike in the situation examined in [24], the BW constituent is engulfed in other contributions and does not have the prominence for allowing a clear identification. These observations cogently demonstrate that the detailed analysis of the field at, and immediately behind, the HW wave-front is a key building block towards inferring a causal counterpart of the leaky-wave propagation.
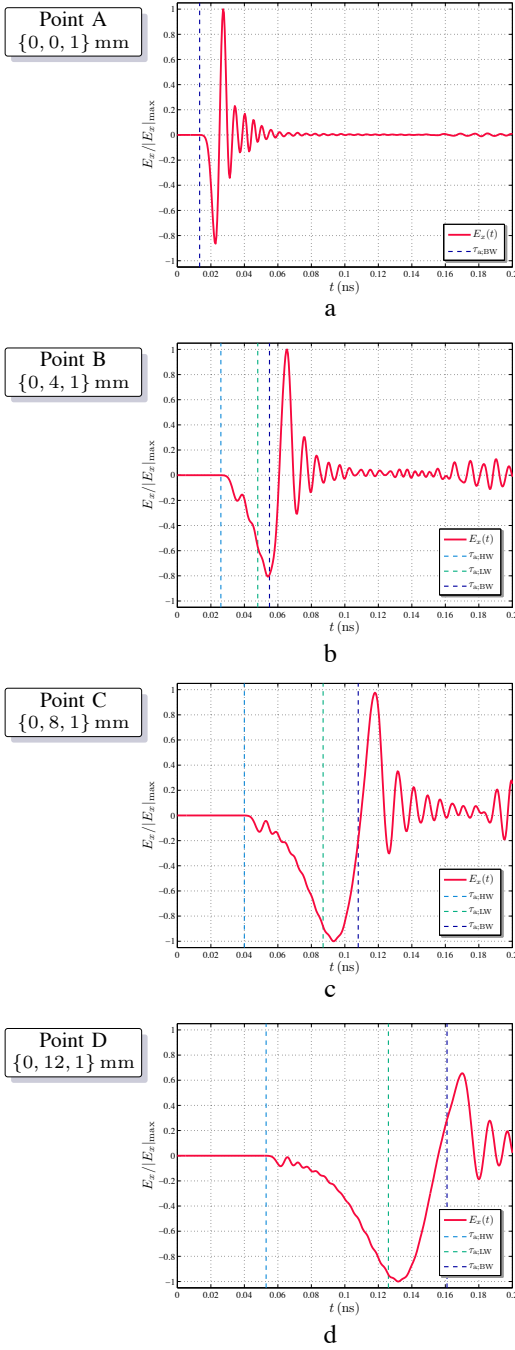
Fig. 4. Simulated responses at the field points A,...,D indicated in Fig. 1 for the $\Delta(t)$ pulse excitation in Fig. 3. The dashed lines correspond to the arrival times of the relevant wave constituents.

V. CONCLUSIONS

The temporal behaviour at the forefront of the pulsed EM field radiated by a long slot in a PEC thin sheet was examined. An interpretation of the HW constituent as the first field disturbance propagating away from the source and sensed at field points located at angles exceeding the critical angle was put forward. The subsequent detailed analysis of the numerically determined signatures at relevant field points allowed singling out features that pave the way towards inferring a causal counterpart of the leaky-wave propagation. In particular, a clear minimum was identified around an arrival time that was previously shown to be associated with a leaky-wave-like behaviour in a somehow related configuration.

APPENDIX

A. Laplace-transform deconvolution method

Assume that

$$y(t) = x(t) \overset{(t)}{*} \Delta(t). \qquad (10)$$

By taking the Laplace transform of this expression and accounting for the Laplace transform

$$\Delta(t) \overset{\text{LT}}{\longmapsto} \hat{\Delta}(s) = [1 - \exp(-st_r)]^2 / (t_r\, s^2) \qquad (11)$$

it is found that the Laplace-transforms $\hat{X}(s)$ and $\hat{Y}(s)$ of $x(t)$ and $y(t)$, respectively, are related as

$$\hat{X}(s) = \frac{\hat{Y}(s)}{\hat{\Delta}(s)} = t_r\, s^2 \frac{\hat{Y}(s)}{[1 - \exp(-st_r)]^2}$$
$$= t_r\, s^2\, \hat{Y}(s) \sum_{n=0}^{\infty} (n+1)\exp(-nst_r) \qquad (12)$$

in which use was made of the geometric series expansion of $(1-x)^{-2}$. By now inverting (12) to the TD, the following deconvolution formula is obtained

$$x(t) = t_r \sum_{n=0}^{\infty} \left[(n+1)\, \partial_t^2 y(t - nt_r) \right]. \qquad (13)$$

This expression is extremely useful since it only requires evaluating $\partial_t^2 y(t - nt_r)$ that may be either obtained analytically or calculated from samples. Moreover, the number of intervening terms is *a priori* known within any finite interval, implying that no supplementary approximation is introduced by the truncation of the series. Nonetheless, the applicability of this strategy is confined to $\Delta(t)$-type excitations.

B. Validation of the conformity between the simulated and deconvolved signatures

The comparison between the original and the deconvolved signatures at all 4 field points are shown in Fig. 5. It is clear that the relevant plots are remarkably consistent. The agreement between the signatures is conclusively demonstrated by calculating the deviation over the interval $\mathcal{T} = \{0 \leqslant t \leqslant 0.2\,(\text{ns})\}$ between pairs of quantities $A(t)$ and $B(t)$ via

$$\text{Dev}_\%(A, B) = \frac{\int_{\mathcal{T}} \left| A_{\text{norm}}(t) - B_{\text{norm}}(t) \right| \text{d}t}{\int_{\mathcal{T}} \left| A_{\text{norm}}(t) \right| \text{d}t} \times 100 \qquad (14)$$

in which A_{norm} and B_{norm} denote the normalised (to their maximum absolute values) versions of A and B, respectively. The largest discrepancy between any two signatures amounted to $5 \cdot 10^{-6}\%$!
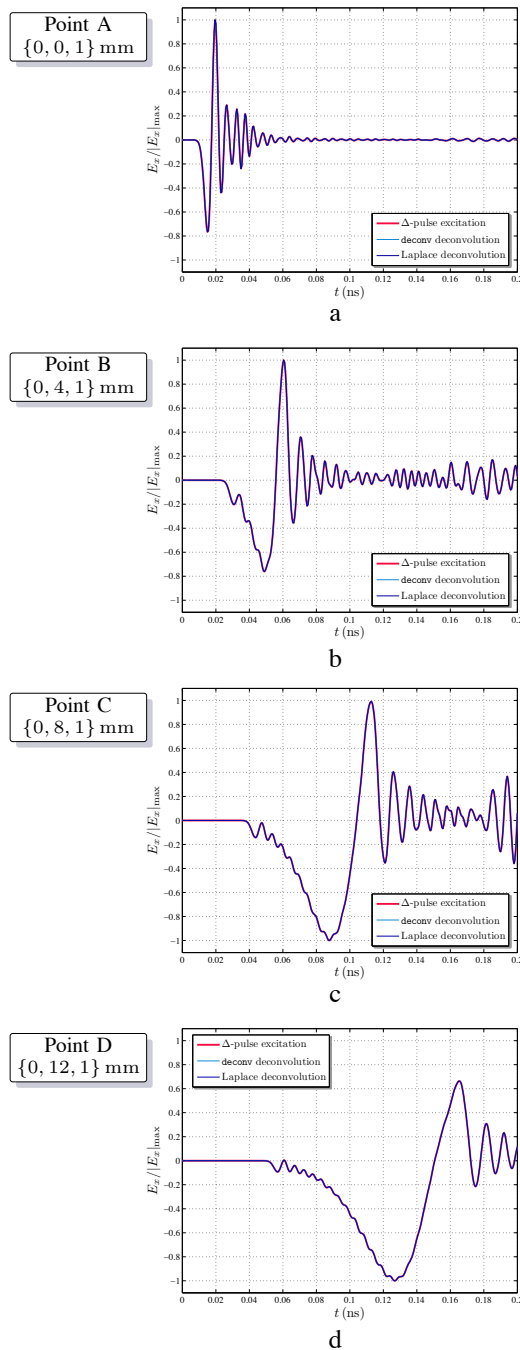
Fig. 5. Comparison of the simulated responses and the corresponding deconvolved signatures at the sampling points indicated in Fig. 1.

REFERENCES

[1] Z. Chen, C. Han, Y. Wu, L. Li, C. Huang, Z. Zhang, G. Wang, and W. Tong, "Terahertz wireless communications for 2030 and beyond: A cutting-edge frontier," *IEEE Commun. Mag.*, vol. 59, no. 11, pp. 66–72, Nov. 2021.

[2] A. Neto, "UWB, non dispersive radiation from the planarly fed leaky lens antenna – Part 1: Theory and design," *IEEE Trans. Antennas Propag.*, vol. 58, no. 7, pp. 2238–2247, Jul. 2010.

[3] N. Llombart, G. Chattopadhyay, A. Skalare, and I. Mehdi, "Novel terahertz antenna based on a silicon lens fed by a leaky wave enhanced waveguide," *IEEE Trans. Antennas Propag.*, vol. 59, no. 6, pp. 2160–2168, Jun. 2011.

[4] N. T. Nguyen, R. Sauleau, and L. Le Coq, "Reduced-size double-shell lens antenna with flat-top radiation pattern for indoor communications at millimeter waves," *IEEE Trans. Antennas Propag.*, vol. 59, no. 6, pp. 2424–2429, Jun. 2011.

[5] I. Vakili, L. Ohlsson, M. Gustafsson, and L.-E. Wernersson "Wideband and non-dispersive wavelet transmission using leaky lens antenna," *Electron. Lett.* vol. 49, no. 5, Feb. 2013. [Online]. https://doi.org/10.1049/el.2013.0005.

[6] A. Neto, N. Llombart, J. J. A. Baselmans, A. Baryshev, and S. J. C. Yates, "Demonstration of the leaky lens antenna at submillimeter wavelengths," *IEEE Trans. THz Sci. Technol.* vol. 4, no. 1, pp. 26–32, Jan. 2014.

[7] L. Ohlsson, D. Sjöberg, and L.-E. Wernersson, "Codesign of compact III-V millimeter-wave wavelet transmitters with on-chip antennas," *IEEE Trans. Microw. Theory Techn.* vol. 66, no. 1, pp. 273–279, Jan. 2018.

[8] Sven van Berkel, E. S. Malotaux, C. De Martino, M. Spirito, D. Cavallo, A. Neto, and N. Llombart, "Wideband double leaky slot lens antennas in CMOS technology at submillimeter wavelengths," *IEEE Trans. THz Sci. Technol.* vol. 10, no. 5, pp. 540–553, Sep. 2020.

[9] R. Guzmán-Quirós, , J. L. Gómez-Tornero, A. R. Weily, and Y. J. Guo, "Electronic full-space scanning with 1-D Fabry-Pérot LWA using electromagnetic band-gap," *IEEE Antennas Wireless Propag. Lett.*, vol. 11, pp. 1426–1429, Feb. 2012.

[10] A. Hosseini, F. Capolino, F. De Flaviis, P. Burghignoli, G. Lovat, and D. R. Jackson, "Improved bandwidth formulas for Fabry-Pérot cavity antennas formed by using a thin partially-reflective surface," *IEEE Trans. Antennas Propag.*, vol. 62, no. 5, pp. 2361–2367, May 2014.

[11] A. Hosseini, F. Capolino, and F. De Flaviis, "Gain enhancement of a V-Band antenna using a Fabry-Pérot cavity with a self-sustained all-metal cap with FSS," *IEEE Trans. Antennas Propag.*, vol. 63, no. 3, pp. 909–921, Mar. 2015.

[12] A. T. Almutawa, A. Hosseini, D. R. Jackson, and F. Capolino, "Leaky-wave analysis of wideband planar Fabry-Pérot cavity antennas formed by a thick PRS," *IEEE Trans. Antennas Propag.*, vol. 67, no. 8, pp. 5163–5175, Aug. 2019.

[13] D. Comite, S. K. Podilchak, M. Kuznetcov, V. Gómez-Guillamón Buendía, P. Burghignoli, P. Baccarelli, and A. Galli, "Wideband array-fed Fabry-Pérot cavity antenna for 2-D beam steering," *IEEE Trans. Antennas Propag.*, vol. 69, no. 2, pp. 784–794, Feb. 2021.

[14] D. R. Jackson, C. Caloz, and T. Itoh, "Leaky-wave antennas," *Proc. IEEE*, vol. 100, no. 7, pp. 2194–2206, Jul. 2012.

[15] F. Monticone and A. Alù, "Leaky-wave theory, techniques, and applications: From microwaves to visible frequencies," *Proc. IEEE*, vol. 103, no. 5, pp. 793–821, May 2015.

[16] A. Neto and S. Maci, "Green's function for an infinite slot printed between two homogeneous dielectrics – Part I: Magnetic currents," *IEEE Trans. Antennas Propag.*, vol. 51, no. 7, pp. 1572–1581, Jul. 2003.

[17] S. Maci and A. Neto, "Green's function for an infinite slot printed between two homogeneous dielectrics – Part II: Uniform asymptotic solution," *IEEE Trans. Antennas Propag.*, vol. 52, no. 3, pp. 666–676, Mar. 2004.

[18] A. T. de Hoop, "A modification of Cagniard's method for solving seismic pulse problems," *Appl. Sci. Res.*, Sect. B, no. 8, pp. 349–356, May 1960.

[19] A. T. de Hoop and H. J. Frankena, "Radiation of pulses generated by a vertical electric dipole above a plane, non-conducting, earth," *Appl. Sci. Res.*, Sect. B, no. 8, pp. 369–377, May 1960.

[20] W. C. Chew, *Waves and Fields in Inhomogeneous Media*, 2nd edition, Piscataway, NJ: IEEE PRESS, 1995.

[21] M. Štumpf, A. T. de Hoop, and G. A. E. Vandenbosch, "Generalized ray theory for time-domain electromagnetic fields in horizontally layered media," *IEEE Trans. Antennas Propag.*, vol. 61, no. 5, pp. 2676–2687, May 2013.

[22] M. Štumpf, *Time-Domain Electromagnetic Reciprocity in Antenna Modeling*. Hoboken, NJ: IEEE Press-Wiley, 2019.

[23] *Metasurface Electromagnetics: The Cagniard-DeHoop time-domain approach*. London, UK: IET, 2022.

[24] M. Štumpf, J. Gu, and I. E. Lager, "Time-domain electromagnetic leaky waves," accepted in *IEEE Trans. Antennas Propag.*.